Satellite Orientation and Position for Geometric Correction of Scanner Imagery

*Paul H. Salamonowicz**
U.S. Geological Survey, Reston, VA 22092

ABSTRACT: The U.S. Geological Survey (USGS) Mini Image Processing System currently relies on a polynomial method for geometric correction of Landsat multispectral scanner (MSS) data. A large number of ground control points are required because polynomials do not model the sources of error. In order to reduce the number of necessary points, a set of mathematical equations modeling the Landsat satellite motions and MSS scanner has been derived and programmed. A best fit to the equations is obtained by using a least-squares technique that permits computation of the satellite orientation and position parameters based on only a few control points. The parameters thus derived serve as a basis for geometric correction of the whole image. A preliminary test shows that the model permits pixel location to be predicted to approximately 100 metres based on six control points.

INTRODUCTION

COMPUTER PROCESSING of remote sensing data is performed for a variety of applications, and often geometric correction of the data is a requirement. One technique commonly used to transform the raw data into a geometrically corrected image is to apply a low-order polynomial correction. Image points whose corresponding ground coordinates are also known (usually from an existing map) are used to fit the data to the ground by means of the polynomial. However, polynomials are not a proper model of the physical phenomena which cause the distortions in the raw image data. Because of this and the fact that polynomials can often numerically "misbehave," 30 to 40 ground control points are often required for satisfactory geometric correction of one Landsat MSS scene. In the last few years several methods have been presented that model the satellite motions and imaging systems, thus reducing the number of control points needed. These methods illustrate the feasibility of correcting an image with only a few ground control points (Sawada *et al.*, 1981; Friedmann *et al.*, 1983). Reducing the number of control points required represents a savings in the time needed for control selection, an effort which is both tedious and a potential source of error. Alternate approaches to this problem are given by Mikhail and Baker (1973) and Paderes and Mikhail (1983).

The U.S. Geological Survey (USGS) Mini Image Processing System (MIPS) was designed as a small office system with the potential of being used in a field environment (Chavez, 1984). Currently the MIPS relies on a polynomial method for geometric processing of MSS data. The objective of this project was to design and program a set of mathematical equations that model the Landsat satellite motions and MSS scanner in such a way that the position and orientation of the satellite may be predicted for each pixel in the image based on only a few ground control points. The derived math model would then form the basis of an alternate MIPS geometric correction procedure for satellite scanner imagery. The mathematical model derived utilizes a circular orbit, which is adequate for most remote sensing satellites (Colwell, 1983) and has the added benefit of allowing for simpler equations.

MATHEMATICAL MODEL

The mathematical model is similar in concept to the photogrammetric collinearity equations, but because of the radically different type of sensor, the details are quite different. Raw MSS data are rectangular images consisting of an array of pixels. Individual pixels are identified by sample number (SN) and line number (LN), as shown in Figure 1. The samples are transverse to the direction of spacecraft motion and sample numbers increase in the direction of the scan. The line numbers increase in the direction of satellite motion.

*Now employed by the Defense Mapping Agency.

PHOTOGRAMMETRIC ENGINEERING AND REMOTE SENSING,
Vol. 52, No. 4, April 1986, pp. 491–499.

0099-1112/86/5204-491$02.25/0

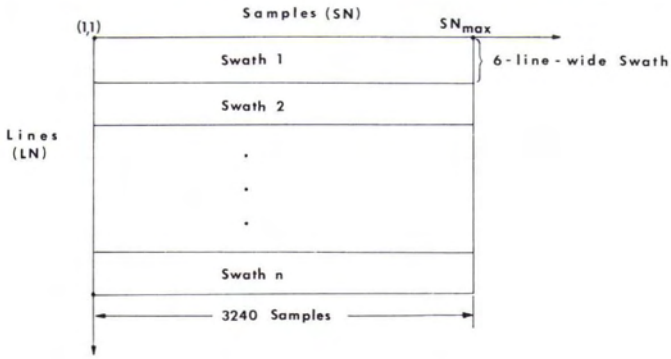

FIG. 1. Landsat multispectral scanner image.

One swath of the MSS is six lines wide and approximately 3,240 samples (the number of samples varies slightly depending upon the particular satellite) long. The MSS images in such a way that succeeding scans leave no gaps in coverage. The center of a pixel can be taken as the point representing the angular field of the pixel. With this assumption, an angular representation of the instantaneous field of view (IFOV) of one pixel is 4.927×10^{-3} degrees, and the angular representation of the cross-track field of view (CTFOV) of the 3,240 samples is 11.56 degrees.

The first step in processing the raw data is to correct the sample positions. Errors in sample position exist because of periodic variations in the scan rate. The corrected sample (SN_{corr}) is computed by applying a polynomial to the raw sample number (SN): that is,

$$SN_{corr} = SN^*(1 + c_1 + SN^*(c_2 + SN^*(c_3 + SN^*c_4))) \quad (1)$$

The coefficients of the polynomial are given by Forrest (1981) as $c_1 = 0.0$, $c_2 = -0.01733$, $c_3 = 1.60403 \times 10^{-5}$, $c_4 = -3.3011 \times 10^{-9}$.

The mathematical model requires a three-dimensional image coordinate system. Because the MSS scene is not a perspective image, a refined coordinate system such as that normally used in analytical photogrammetry problems cannot be defined. However, using the IFOV and CTFOV values in conjunction with the image scan dimensions (that is, six lines by 3,240 samples), a dimensionless (X, Y, Z) image space coordinate system can be constructed. The approach used in defining the image coordinate system is based on that developed by Sawada (Sawada *et al.*, 1981) and is described briefly as modified for this project.

The image space coordinate system is constructed by erecting the $+z$ vector at the center of a particular scan, along the normal to the image and pointing away from Earth, $+x$ in the direction of spacecraft travel, and $+y$ in the direction that results in a right-hand coordinate system (Figure 2). The origin is an arbitrary unit length above the center of the scan. Direction angles ψ and θ, in the x and y directions, respectively, can be computed from line numbers (LN) and sample numbers (SN_{corr}) by

$$\psi = (-7/2 + LN - [(LN-1)/LN_{max}]^*LN_{max})^*IFOV \quad (2)$$

$$\theta = ((1/(SN_{max}-1))^*(SN_{corr}-1) - 1/2)^*CTFOV \quad (3)$$

LN_{max} is the maximum number of lines per scan, in this case six, and SN_{max} is 3,240. In both Equation 2 and in Equation 4 below, the computation $(LN\text{-}1)/LN_{max}$ is carried out in integer arithmetic. Because the scan rate correction coefficients, sampling interval (S_{int}), and scan period (T) are known, the elapsed time, t, since the start of imaging can be computed by

$$t = [(LN\text{-}1)/LN_{max}] * T + (SN_{corr} - 1) * S_{int} \quad (4)$$

Thus, a time value is associated with each pixel. This time information is not utilized in constructing the image space coordinates but is logically computed at this point because line and sample are not referenced once the computations shown in Equations 2, 3, and 4 are completed.

If a principal distance of 1 is assumed, a rectangular image space coordinate system can be formed. However, these coordinates are at an arbitrary scale. The vector from the origin to the pixel of the ground control point in the image space system is **p**. The normalized components are defined by

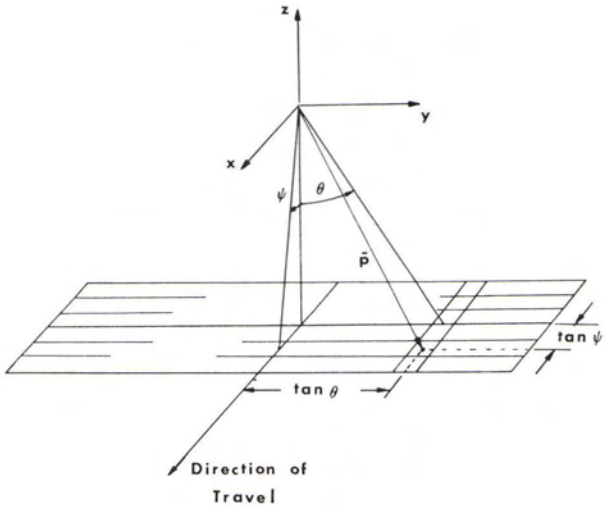

FIG. 2. Image coordinate system.

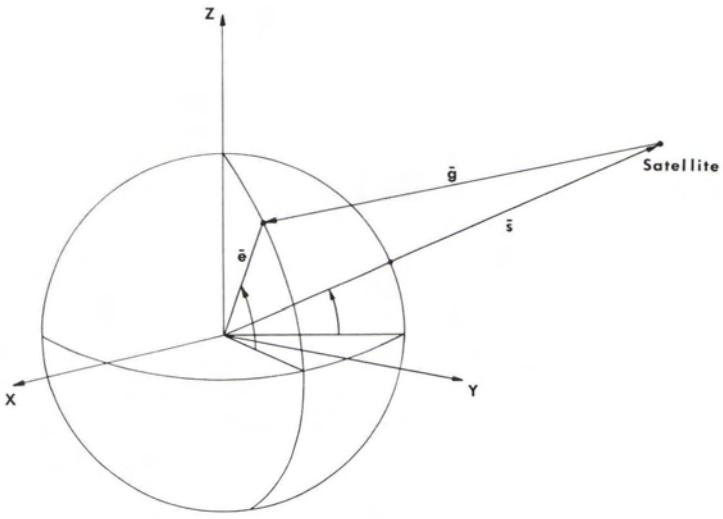

FIG. 3. Fundamental observation triangle.

$$\begin{aligned} x_p &= 1\ (\tan \psi)/n = (\tan \psi)/n \\ y_p &= 1\ (\tan \theta)/n = (\tan \theta)/n \\ z_p &= 1/n \end{aligned} \tag{5}$$

where $n = [\tan^2 \psi + \tan^2 \theta + 1]^{1/2}$

With the image coordinates defined, attention can now be turned to the location of the satellite in relation to the Earth, that is, the object space. One condition utilized in defining the position of the satellite in object space is that referred to as the Fundamental Observation Triangle (FOT) (Slama, 1980). The FOT (Figure 3) illustrates the relationship

$$\mathbf{s} - \mathbf{e} = -\mathbf{g} \tag{6}$$

The vector **s** is the positional vector of the satellite in an Earth-centered coordinate system; **e** is the positional vector of a ground control point in the same coordinate system, with geodetic latitude ϕ_e,

longitude λ_e, and height h, which has been imaged at the time when the satellite's position is given by **s**. The Earth-centered coordinates are geocentric coordinates; however, it is important to realize that the inertial position of the geocentric system changes because of the Earth's rotation. Such a coordinate system is not suitable for the mathematical model being described. Instead, the geocentric coordinate system fixed at the time of imaging the first control point is defined to be the Earth-centered coordinate system used in this study and shall be referred to as the modified geocentric coordinate system. The only computation required to effect this system is the correction of each control point longitude for the Earth's rotation. In general, for the i^{th} ground control point, the longitude correction is given by

$$\lambda_c = w_e (t_i - t_1) \tag{7}$$

w_e is the Earth rotation rate and t_i and t_1 are the elapsed times of imaging for the i^{th} control point and the first control point, respectively, as given by Equation 4. The corresponding satellite longitudes require no correction because, as will be shown later, they are computed as a function of other orbital elements and do not inherently include Earth rotation.

The position vector of the satellite, **s**, at some instant has geocentric latitude ϕ_s, longitude λ_s, and orbital radius R_s and has modified geocentric coordinates given by

$$\mathbf{s} = \begin{bmatrix} X_s \\ Y_s \\ Z_s \end{bmatrix} = \begin{bmatrix} R_s \cos \phi_s \cos \lambda_s \\ R_s \cos \phi_s \sin \lambda_s \\ R_s \sin \phi_s \end{bmatrix} \tag{8}$$

Modified geocentric coordinates also may be defined for **e**, with parameters as given earlier. For a given Earth equatorial radius, a, and an eccentricity, ϵ, **e** has coordinates

$$\mathbf{e} = \begin{bmatrix} X_e \\ Y_e \\ Z_e \end{bmatrix} = \begin{bmatrix} (a/(1 - \epsilon^2 \sin^2 \phi_e)^{1/2} + h) \cos \phi_e \cos(\lambda_e + \lambda_c) \\ (a/(1 - \epsilon^2 \sin^2 \phi_e)^{1/2} + h) \cos \phi_e \sin(\lambda_e + \lambda_c) \\ (a(1 - \epsilon^2)) \sin \phi_e/(1 - \epsilon^2 \sin^2 \phi_e)^{1/2} + h \sin \phi_e \end{bmatrix} \tag{9}$$

The satellite position may also be characterized in terms of orbital parameters: inclination (I_s), longitude of descending node (α_s), orbit radius (R_s), and geocentric latitude (ϕ_s) (Figure 4). Noting that $|\mathbf{s}| = R_s$, the satellite tangential velocity can be computed by

$$v_s = (GM/R_s)^{1/2} \tag{10}$$

GM is the product of the constant of gravitation and the mass of the Earth (Alexander, 1983). If the initial geocentric latitude, ϕ_{s_0}, is defined to be that geocentric latitude of the satellite at the time that the first ground control point is imaged, then the instantaneous satellite geocentric latitude, longitude, and azimuth, denoted by ϕ_s, λ_s, and Az_s, respectively, can be computed as

$$\begin{aligned} \phi_s &= \phi_{s_0} - \tan^{-1}[\tan (v_s(t_i - t_1)/R_s) \cos(\sin^{-1}(-\cos I_s/\cos \phi_{s_0}))] \\ \lambda_s &= \alpha_s + \sin^{-1}(\tan \phi_s/\tan (\pi - I_s)) \\ Az_s &= \sin^{-1}(-\cos I_s/\cos \phi_s) + \pi/2 \end{aligned} \tag{11}$$

Returning to the FOT, a rotation matrix, (**R**), that is a function of instantaneous satellite nadir latitude and longitude, and instantaneous azimuth, can be defined such that, when (**R**) is applied to the modified geocentric coordinate system, it rotates the modified geocentric system to the satellite nadir system (Figure 4). Using the shorthand notation s( ) and c( ) to represent sine and cosine, the rotation matrix, (**R**), has elements

$$\begin{aligned} r_{11} &= s(Az_s)\, s(\phi_s)\, c(\lambda_s) - c(Az_s)\, s(\lambda_s) \\ r_{12} &= s(Az_s)\, s(\phi_s)\, s(\lambda_s) + c(Az_s)\, c(\lambda_s) \\ r_{13} &= -s(Az_s) c(\phi_s) \\ r_{21} &= -c(Az_s)\, s(\phi_s)\, c(\lambda_s) - s(Az_s)\, s(\lambda_s) \\ r_{22} &= -c(Az_s)\, s(\phi_s)\, s(\lambda_s) + s(Az_s)\, c(\lambda_s) \\ r_{23} &= c(Az_s)\, c(\phi_s) \\ r_{31} &= c(\phi_s)\, c(\lambda_s) \\ r_{32} &= c(\phi_s)\, s(\lambda_s) \\ r_{33} &= s(\phi_s) \end{aligned} \tag{12}$$

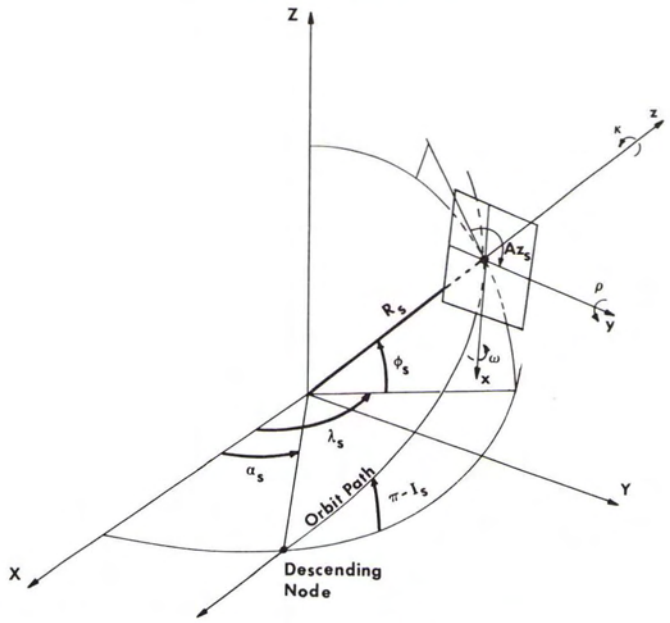

FIG. 4. Satellite orbital elements.

Applying (**R**) to Equation 6 yields

$$(\mathbf{R})\ (\mathbf{s} - \mathbf{e}) = -\ (\mathbf{R})\ \mathbf{g} \tag{13}$$

Further motions that affect the image are the rolling, pitching, and yawing of the satellite. Assuming the satellite has initial roll, pitch, and yaw, denoted by ω_o, ρ_o, and κ_o, respectively, and roll, pitch, and yaw rates, as denoted by $\dot{\omega}$, $\dot{\rho}$, $\dot{\kappa}$, respectively, the instantaneous roll, pitch, and yaw for the i^{th} point are defined by

$$\begin{aligned} \omega_s &= \omega_o + \dot{\omega}(t_i - t_1) \\ \rho_s &= \rho_o + \dot{\rho}(t_i - t_1) \\ \kappa_s &= \kappa_o + \dot{\kappa}(t_i - t_1) \end{aligned} \tag{14}$$

An orientation matrix, (**M**), that is a function of roll, pitch, and yaw, can be defined such that when (**M**) is applied to a set of satellite nadir coordinates, it rotates them to the instantaneous satellite coordinates, that is, to the image space coordinates of the scanner (Figure 2). The orientation matrix, (**M**), has elements

$$\begin{aligned} m_{11} &= c(\kappa_s)\ c(\rho_s) \\ m_{12} &= s(\omega_s)\ s(\rho_s)\ c(\kappa_s) + c(\omega_s)\ s(\kappa_s) \\ m_{13} &= -c(\omega_s)\ s(\rho_s)\ c(\kappa_s) + s(\omega_s)\ s(\kappa_s) \\ m_{21} &= -s(\kappa_s)\ c(\rho_s) \\ m_{22} &= -s(\omega_s)\ s(\rho_s)\ s(\kappa_s) + c(\omega_s)\ c(\kappa_s) \\ m_{23} &= c(\omega_s)\ s(\rho_s)\ s(\kappa_s) + s(\omega_s)\ c(\kappa_s) \\ m_{31} &= s(\rho_s) \\ m_{32} &= -s(\omega_s)\ c(\rho_s) \\ m_{33} &= c(\omega_s)\ c(\rho_s) \end{aligned} \tag{15}$$

Applying (**M**) to Equation 13 yields

$$(\mathbf{M})\ (\mathbf{R})\ (\mathbf{s} - \mathbf{e}) = -\ (\mathbf{M})\ (\mathbf{R})\ \mathbf{g} \tag{16}$$

The vector represented by Equation 16 now has the same direction cosines as the image space coordinates. The only difference between the vectors represented by Equations 16 and 5 is that of vector length. **p** and

the vector described by Equation 16 differ by a factor of $|\mathbf{g}|$. Dividing Equation 16 by $|\mathbf{g}|$ and equating Equations 5 and 16 yields, after rearranging and expanding,

$$\begin{bmatrix} x_p \\ y_p \\ z_p \end{bmatrix} = -\frac{(\mathbf{M})\,(\mathbf{R})}{|\mathbf{g}|}\begin{bmatrix} X_s - X_e \\ Y_s - Y_e \\ Z_s - Z_e \end{bmatrix} \tag{17}$$

The vector length, $|\mathbf{g}|$, is an unknown which will be different for each control point. However, this parameter can be eliminated. For clarity, let the product (**M**) (**R**) be defined by

$$\mathbf{U} = (\mathbf{M})\,(\mathbf{R}) \tag{18}$$

where **U** has elements $u_{11}, u_{12}, \ldots, u_{33}$
and let k be a constant defined by

$$k = \frac{1}{|\mathbf{g}|} \tag{19}$$

The equations in 17 can be expanded and, upon substitution of Equations 18 and 19, will yield the expressions

$$\begin{aligned} x_p &= -k(u_{11}(X_s - X_e) + u_{12}(Y_s - Y_e) + u_{13}(Z_s - Z_e)) \\ y_p &= -k(u_{21}(X_s - X_e) + u_{22}(Y_s - Y_e) + u_{23}(Z_s - Z_e)) \\ z_p &= -k(u_{31}(X_s - X_e) + u_{32}(Y_s - Y_e) + u_{33}(Z_s - Z_e)) \end{aligned} \tag{20}$$

Now, if the x and y expressions of Equation 20 are divided by the z expression, the constant k is eliminated. Once the division is carried out, and after some algebraic manipulations, the three expressions in Equation 20 can be reduced to two expressions of the form

$$\begin{aligned} F_x &= x_p - z_p\frac{u_{11}(X_s - X_e) + u_{12}(Y_s - Y_e) + u_{13}(Z_s - Z_e)}{u_{31}(X_s - X_e) + u_{32}(Y_s - Y_e) + u_{33}(Z_s - Z_e)} = 0 \\ F_y &= y_p - z_p\frac{u_{21}(X_s - X_e) + u_{22}(Y_s - Y_e) + u_{23}(Z_s - Z_e)}{u_{31}(X_s - X_e) + u_{32}(Y_s - Y_e) + u_{33}(Z_s - Z_e)} = 0 \end{aligned} \tag{21}$$

Two expressions of the type given in Equation 21 can be written for each control point. Therefore, a system of $2n$ equations results from n control points. The quantities x_p, y_p, z_p, X_e, Y_e, and Z_e in Equation 21 are known. The quantities X_s, Y_s, Z_s, and $u_{11}, u_{12}, \ldots, u_{33}$ are functions of several unknown independent parameters. These parameters are the satellite radius vector, inclination, longitude of the descending node, initial latitude at the time of imaging the first ground control point, roll, pitch, yaw, roll rate, pitch rate, and yaw rate. It is required that enough control points be used such that the $2n$ system of equations is overdetermined. Then a least-square adjustment technique, discussed in the following section, may be used to solve the system for the set of unknown parameters so that the observation residuals are minimized.

ADJUSTMENT

The condition equations developed in the mathematical model are functions of several independent parameters for which only approximate values are known. The goal of the adjustment is to determine these parameters more accurately. The adjustment procedure has been designed to allow the computation of attitude rates to be optional and to permit two methods of solution.

In some circumstances the computation of attitude rates may be unnecessary. The adjustment procedure has been designed so that the computation of attitude rates can be held at 0°/sec and not adjusted. In this case four ground control points are the minimum number required for solution. Four control points, however, provide only one redundancy. If the attitude rates are allowed to adjust, then five points are the minimum necessary, but they provide no redundancies. Therefore, six control points providing two redundancies are considered the minimum control requirement for computing attitude rates.

If *a priori* information about the satellite parameters is known and this information is considered reliable, it may be desirable to weight the parameters by means of *a priori* standard deviations rather than permit free adjustment. The software has been designed to allow, as an option, the weighting of the parameters by means of *a priori* standard deviations. This technique uses the unified approach to least-squares ad-

justment described by Mikhail (1976). In this case, the corrections to the estimates of the parameters are computed by

$$\triangle_i = [\mathbf{B}^T(\mathbf{AQA}^T)^{-1}\,\mathbf{B} + \mathbf{W}_{xx}]^{-1}\,\mathbf{B}^T(\mathbf{AQA}^T)^{-1}\,(\underline{\mathbf{f}} - \mathbf{W}_{xx}\,\underline{\mathbf{f}}_x). \tag{22}$$

$\triangle_i$ is the unknown parameter correction vector for the i^{th} iteration.
A is defined by

$$\mathbf{A} = \begin{bmatrix} \mathbf{A}_1 & & \bigcirc \\ & \mathbf{A}_2 & \\ \bigcirc & & \mathbf{A}_n \end{bmatrix} \tag{23}$$

where $\mathbf{A}_j$ ($j = 1$ to n, the number of points) is a 2 by 2 matrix of partial derivatives of the condition equations (Equation 21) with respect to the observations, x_p and y_p, for point j such that

$$\mathbf{A}_j = \begin{bmatrix} \dfrac{\partial F_{xj}}{\partial_{x_P}} & \dfrac{\partial F_{xj}}{\partial_{y_P}} \\ \dfrac{\partial F_{yj}}{\partial_{x_P}} & \dfrac{\partial F_{yj}}{\partial_{y_P}} \end{bmatrix} \tag{24}$$

B is defined by

$$\mathbf{B} = [\mathbf{B}_1\ \mathbf{B}_2 \ldots \mathbf{B}_n]^T \tag{25}$$

where $\mathbf{B}_j$ ($j = 1$ to n, the number of points) is either a 2 by 7 or 2 by 10 matrix (depending upon the selection of the option to compute attitude rates) of partial derivatives of the two condition equations (Equation 21) with respect to the unknown parameters for point j such that

$$\mathbf{B}j = \begin{bmatrix} \dfrac{\partial F_{xj}}{\partial \omega_s} \dfrac{\partial F_{xj}}{\partial \rho_s} \dfrac{\partial F_{xj}}{\partial \kappa_s} \dfrac{\partial F_{xj}}{\partial \phi_{s_O}} \dfrac{\partial F_{xj}}{\partial \alpha_s} \dfrac{\partial F_{xj}}{\partial I_s} \dfrac{\partial F_{xj}}{\partial R_s} \dfrac{\partial F_{xj}}{\partial \dot{\omega}_s} \dfrac{\partial F_{xj}}{\partial \dot{\rho}_s} \dfrac{\partial F_{xj}}{\partial \dot{\kappa}_s} \\ \\ \dfrac{\partial F_{yj}}{\partial \omega_s} \dfrac{\partial F_{yj}}{\partial \rho_s} \dfrac{\partial F_{yj}}{\partial \kappa_s} \dfrac{\partial F_{yj}}{\partial \phi_{s_O}} \dfrac{\partial F_{yj}}{\partial \alpha_s} \dfrac{\partial F_{yj}}{\partial I_s} \dfrac{\partial F_{yj}}{\partial R_s} \dfrac{\partial F_{yj}}{\partial \dot{\omega}_s} \dfrac{\partial F_{yj}}{\partial \dot{\rho}_s} \dfrac{\partial F_{yj}}{\partial \dot{\kappa}_s} \end{bmatrix} \tag{26}$$

f if a vector representing the evaluation of Equation 21 at the current estimate of the unknowns. **Q** is a diagonal matrix containing the inverse of the squares of the *a priori* standard deviations of the observations; $\mathbf{W}_{xx}$ is the parameter weight matrix based on the inverse square of the *a priori* standard deviations of the parameters, and $\mathbf{f}_x$ is the vector sum of the correction vectors of the previous $(i-1)$ iterations.

If, however, it is desired to let the parameters adjust freely, the correction vector for the i^{th} iteration is simply computed by the method of adjustment of indirect observations (Mikhail, 1976). The correction vector is

$$\triangle_i = [\mathbf{B}^T(\mathbf{AQA}^T)^{-1}\,\mathbf{B}]^{-1}\,\mathbf{B}^T\,(\mathbf{AQA}^T)^{-1}\,\mathbf{f} \tag{27}$$

Here no $\mathbf{W}_{xx}$ or $\mathbf{f}_x$ appear, and all other symbols are as previously defined.

The *a priori* standard deviations used in defining the **Q** and $\mathbf{W}_{xx}$ matrices must be supplied by the user on a case-by-case basis. Inspection of Equations 23 and 24 shows that **A** is the identity matrix.

Because the Landsat MSS imagery is geometrically weak, the possibility of the normal equations being ill conditioned is greatly increased. In order to minimize the influence of round-off error, which could be greatly magnified by any ill conditioning, the numerical reduction scheme includes a pivoting algorithm and, as an option, the normal equations may be scaled (for details, see Jennings (1977), Stewart (1973), and Forsythe and Moler (1967)).

EXPERIMENTAL RESULTS AND ANALYSIS

A preliminary experiment was carried out to test the programmed equations. Using a Landsat MSS scene over the northern part of Iowa, 13 points, identifiable on both the image and existing maps, were selected. Pixel line and sample numbers of each point were estimated using a print of the raw MSS scene on which a grid was superimposed over every tenth line and sample. The line and sample of a map-identifiable image point could then be estimated to within a pixel. This gridded image was produced on the MIPS at the USGS Flagstaff facility. Corresponding latitudes, longitudes, and elevations were obtained from existing USGS quadrangles. Of the 13 points selected, six well-distributed points were used as the ground control, while the remaining seven points served as test points (Figure 5). Once the satellite parameters were determined from the least-squares adjustment based on the six ground control points, the pixel line and

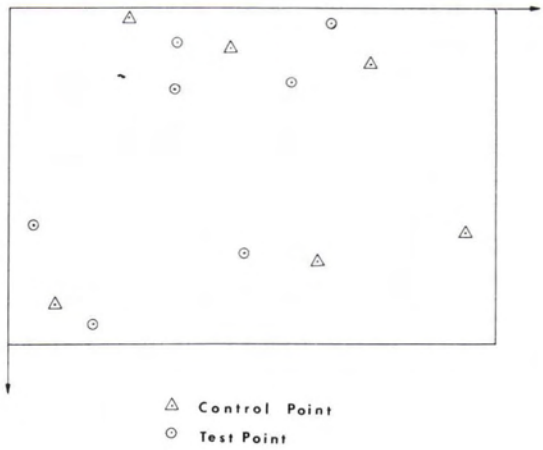

FIG. 5. Control and test point locations.

TABLE 1. COMPARISON OF COMPUTED PARAMETERS AND NOMINAL LANDSAT 1 VALUES

Parameter	Computed Value	Nominal Landsat 2 Value*
Roll (deg)	−1.54	0 ± 1.0
Pitch (deg)	1.39	0 ± 0.7
Yaw (deg)	3.99	0 ± 1.0
Initial latitude (deg)	43.59	N/A
Longitude of descending node (deg)	253.75	N/A
Inclination (deg)	101.77	99.2
Roll rate (deg/sec)	0.025	0.0
Pitch rate (deg/sec)	0.002	0.0
Yaw rate (deg/sec)	0.008	0.0
Orbit radius (km)	7286.68	7285.99 (semi-major axis)

*(USGS, 1979)

sample numbers of each of the 13 points were projected to the surface of the Earth using the computed parameters. Because the MSS scene is a non-stereo image, an elevation must be assumed in order to project the points down to the Earth's surface. The software allows for two options: the user may supply the elevation of the datum, or the program will use the average elevation of the control points. The mathematical algorithm used to project the points to the Earth's surface is that described by Puccinelli (1976).

Once projected down to the Earth, the computed positions were compared to the known planimetric positions. The root-mean-square errors (RMSE) of position of the six control points was 7.3 metres. The RMSE of position of the seven test points was 93.1 metres. For the particular test image, the option to compute attitude rates was specified and the average elevation of the control points was used as the elevation datum. The computed parameters are compared, where applicable, with nominal values for Landsat 2 in Table 1. Initially it was intended to test the computations with both fixed and adjustable attitude rates. However, when the attitude rates were fixed, the solution oscillated but never converged.

The close fit of the ground control was expected because these points were used to determine the parameters. The RMSE of the test points indicates the true accuracy of the system, and for the preliminary test image the fit is under two pixels; however, this value may be a conservative indication of the accuracy, because the only features on the test image that were suitable for use as control and test points were water features, such as stream intersections and points of land jutting out into lakes. Such features are subject to change due to a variety of factors; because the dates on the maps and the date of the image differ by several years, it is quite possible that some variation in positions of the features exists. Testing with an image with more well-defined cultural features will help determine whether or not the solution was affected by possible errors in the control.

The reliability of the computed parameters (Table 1) is difficult to assess because no specific Landsat orbit data are available. Based on computations performed with perturbations applied to the control points, the algorithm appears to be sensitive to errors in the control. The perturbation analysis showed that significant variations in the computed parameters were caused by introducing perturbations of several pixels in the control. It is likely that the weak geometry of the imaging system accounts for the sensitivity of the algorithm to such perturbations and, hence, to any errors in the control. This implies that the modeled parameters are, to some extent, absorbing errors which are not fully accounted for by the model. It should also be noted that the distribution of control can have a significant impact on a model such as the one utilized. The pixel identification method may also contribute some error; however, this method has been used successfully in the past.

CONCLUSIONS AND FUTURE CONSIDERATIONS

Based on the preliminary experimental results, the technique used in this project looks promising. Further testing is to be performed with an image having more well-defined features and, therefore, a larger number of more accurate control and test points; it is hoped that the resulting RMSE of position of the test points will be decreased. Testing with such an image will also aid in determining whether denser control can improve the results. The usefulness of extending the scope of the mathematical model will also be examined. In view of the fact that attitude rate computation appears to be required, it may also be necessary to model the effect of attitude accelerations. Also, experiments will be performed to determine whether or not long arcs of MSS imagery along the same orbit can be used to bridge areas of sparse control. Because Landsat MSS imagery is continuous along an orbit, a long continuum of imagery from the same orbit can be treated in the same way as the more typical individual Landsat scene. If such a scheme proves successful, it could be of benefit in a variety of image mapping applications.

REFERENCES

Alexander, J.C., 1983. *Introductory notes on satellite geodesy and orbit analysis*. Privately published.

Chavez, P., 1984. *U.S. Geological Survey Mini Image Processing System (MIPS)*. U.S. Geological Survey Open-File Report 84-880, 12 p.

Colwell, R.N. (ed.), 1983. *Manual of Remote Sensing*, 2nd ed., Vol. I, ch. 16. American Society of Photogrammetry, Falls Church, Va., pp. 699–717.

Forsythe, G., and C.B. Moler, 1967. *Computer Solution of Linear Algebraic Systems*. Prentice Hall, Englewood Cliffs, N.J., pp. 27–48.

Forrest, R.B., 1981. Simulation of orbital image-sensor geometry. *Photogrammetric Engineering and Remote Sensing*, Vol. 47, No. 8, pp. 1187–1193.

Friedmann, D.E., J.P. Friedel, K.L. Magnussen, R. Kwok, and S. Richardson, 1983. Multiple scene precision rectification of spaceborne imagery with very few ground control points. *Photogrammetric Engineering and Remote Sensing*, Vol. 49, No. 12, pp. 1657–1667.

Jennings, A., 1977. *Matrix Computation for Engineers and Scientists*. John Wiley & Sons, New York, N.Y., pp. 100–116.

Mikhail, E.M., 1976. *Observations and Least Squares*. IEP 1976, New York, N.Y.

Mikhail, E.M., and J.R. Baker, 1973, Geometric Aspects in Digital Analysis of Multi-Spectral Scanner (MSS) Data, *Proceedings of the American Society of Photogrammetry*, 39th Annual Meeting, pp. 528–562.

Paderes, F.C., and E.M. Mikhail, 1983, Photogrammetric Aspects of Satellite Imageries, *Technical Papers ACSM-ASP Fall Convention*, Salt Lake City, Utah, pp. 626–635.

Puccinelli, E.F., 1976. Ground location of satellite scanner data. *Photogrammetric Engineering and Remote Sensing*, Vol. 42, No. 4, pp. 537–543.

Sawada, N., M. Kidode, H. Shinoda, H. Asada, M. Iwanaga, S. Watanabe, and K-I Mori, 1981. An analytic correction method for satellite MSS geometric distortion. *Photogrammetric Engineering and Remote Sensing*, Vol. 47, No. 8, pp. 1195–1203.

Slama, C.C. (ed.), 1980. *Manual of Photogrammetry*, 4th ed., ch. 17. American Society of Photogrammetry, Falls Church, Va., pp. 906–915.

Stewart, G.W., 1973. *Introduction to Matrix Computations*. Academic Press, New York, N.Y., pp. 131–158.

U.S. Geological Survey, 1979. *Landsat Data Users Handbook*.

(Received 11 July 1985; accepted 17 October 1985)